Corner states in second order acoustic topological insulator as bound states in the continuum

Ze-Guo Chen[1], Changqing Xu[1], Rasha Al Jahdali[1], Jun Mei[2,*] and Ying Wu[1,*]

[1]*King Abdullah University of Science and Technology (KAUST),Division of Computer, Electrical and Mathematical Science and Engineering (CEMSE), Thuwal 23955-6900, Saudi Arabia*

[2]*Department of Physics, South China University of Technology, Guangzhou 510640, China*

A second order topological insulator is designed on a platform of a two-dimensional (2D) square lattice with all coupling coefficients being positive. Simulated results show the existence of two types of nontrivial corner states in this system, with one type being identified as bound states in the continuum (BIC). The non-BIC corner states are also found by surrounding a nontrivial sample with a trivial one, and interestingly, these perfectly confined corner states can be gradually delocalized and merge into edge states by tuning the inter-system coupling coefficient. Both BIC and non-BIC corner states are originated from bulk dipole moments rather than the quantized quadrupole moments, with the corresponding topological invariant being the 2D Zak phase. Full wave simulations based on realistic acoustic waveguide structures are demonstrated. Our proposal provides an experimentally feasible platform for the study of interplay between BIC and high order topological insulator, and evolution from corner states to edge states.

Topology, a mathematical concept, was introduced to physics along with the discovery of the quantum Hall effect [1-3]. This concept has attracted growing attention accompanying the developments of various topological effects, including quantum spin Hall effect [4,5]and quantum valley Hall effect [6,7]. Recently, some other topological materials, such as Floquet topological insulators and topological crystalline insulators, were proposed and studied[8-12]. A key characteristic of a topological material is the existence of gapless edge states on its boundary, which are immune to defects and impurities as long as the corresponding symmetry is preserved, leading to robust unidirectional transport of electrons without backscattering. Thus, it had been believed that a *d*-dimensional nontrivial material should host (*d-1*)-dimensional gapless edge states on its boundary, until the so-called higher order topological insulators (HOTI) was found very recently [13-17]. It turns out that a *d*-dimensional topological insulator does not necessarily possess (*d-1*)-dimensional edge state, alternatively it can support (*d-n*)-dimensional boundary

states. For example, a two-dimensional (2D) second order topological insulator does not exhibit one- dimensional (1D) gapless edge states, but hosts nontrivial zero-dimensional (0D) corner states. Several tight-binding models, considering quantized quadrupole and octupole moments, have been proposed as candidates for HOTI [13,18], and the attention has soon been extended to the platforms of classical waves including electromagnetic [19-21], acoustics [22-24] and mechanical waves [25] due to their flexibility in adjusting the geometries and potentials.

As another emerging interesting topic in wave propagation, the bound states in continuum (BIC) refer to localized and non-radiative modes whose frequencies are embed in the continuous spectrum of radiating waves [26]. The physical mechanism behind this somehow counter-intuitive phenomenon is diverse , and the prohibited radiation may be attributed to the symmetry mismatch [27] or decoupling through separability [28], or due to an interference effect between multiple radiation channels [29,30]. The ultrahigh quality factor of the BIC is unique and highly desirable for large-area high-power applications including lasing [31-33], sensing [34,35], filtering [36], and nonlinearity enhancement [26].

In this work, we study both the topologically nontrivial corner states and the BIC. We demonstrate that these two seemly unrelated topics could be combined naturally in a simple 2D system. We focus on a special kind of corner states which are simultaneously BIC and nontrivial boundary states of a HOTI. Physical properties of the corner states are studied and explored in realistic acoustic waveguide structures both analytically from a tight binding model and numerically by full wave simulations. Interestingly, in the same platform we also identify the existence of the non-BIC corner states of a second order HOTI. The evolution and transition between these two types of corners states can be realized by tuning the intersystem coupling coefficient. Different from the previously reported works [13,25], the proposed 2D system in our work does not rely on the introduction of a negative hoppling amplitude for the realization of a HOTI. Although both of them are characterized by the 2D Zak phase, their origins of are intrinsically different: the corner states studied here are strongly related to the bulk dipole moments [21,23], while the corner states reported in Ref. [13] are due to the quantized quadruple moments.

The PC considered here is a 2D square lattice composed of rings and waveguides filled with air. As illustrated in Fig. 1(a), the unit cell with lattice constant $a = 4m$ contains four identical

hollow rings with inner and outer radii as $r_0 = 0.35m$ and $r_1 = 0.5m$. Each ring is connected to its nearest neighbors by four rectangular waveguides. The acoustic wave propagates inside the network of these rings and waveguides. Its pressure field φ satisfies the governing equation$[\nabla^2 + \omega^2/c^2]\varphi(\vec{r},\omega) = 0$, where c is the sound velocity in air and the boundaries of the rings and waveguides are treated as hard walls.

The adjacent rings are correlated only through the wave guides, suggesting that the rings and waveguides effectively act as sites and coupling, respectively, in the picture of tight binding [37,38]. In the low frequency regime, the hopping amplitude (i.e., coupling coefficient) between two neighboring rings is proportional to the width of the waveguides, because only fundamental modes can survive inside the waveguides. The intracell and intercell hopping amplitudes are denoted as w and v, respectively, and they can be realized in a realistic PC structure by waveguides with different widths [39,40]. For such a PC system, in the momentum space, the Hamiltonian can be written as

$$H(k) = \begin{pmatrix} \varepsilon_s & -w - ve^{-ik_x a} & -w - ve^{-ik_y a} & 0 \\ -w - ve^{ik_x a} & \varepsilon_s & 0 & -w - ve^{-ik_y a} \\ -w - ve^{ik_y a} & 0 & \varepsilon_s & -w - ve^{-ik_x a} \\ 0 & -w - ve^{ik_y a} & -w - ve^{ik_x a} & \varepsilon_s \end{pmatrix}, \quad (1)$$

where ε_s is the onsite energy (or eigenfrequency) of each ring. Let us consider two different configurations of the unit cells. Configuration A has the hopping amplitudes $w = 5v$, and configuration B has $v = 5w$. As shown in Fig. 1(a), these two configurations can be simulated in PC systems by setting the corresponding waveguide widths as $d_w = 0.05m$ and $d_v = 0.01m$(for configuration A), and $d_w = 0.01m$ and $d_v = 0.05m$ (for configuration B), respectively. Obviously, periodically repeating these unit cells in the 2D space would eventually give rise to two identical PCs that share the same band structure. Both the simulation results obtained from the finite element method (black dots) and the calculation results by the tight-binding model (red curves) are plot in Fig. 1(b), and they agree with each other very well. Detailed fitting parameters for the tight-binding model are given in Ref. [41].

Although configurations A ($w = 5v$) and B ($v = 5w$) share the identical band structure, they are topologically inequivalent. Inspired by the well-known 1D SSH model, one can simply guess that at the critical point $w = v$ [42], where the band gap closes, topological phase transition occurs.

To rigorously characterize the topological phase transition, we need to calculate the corresponding topological index or invariant. Here the relevant topological invariant is the 2D Zak phase or 2D polarization, which is defined as the integral of the Berry connection through [43]

$$\mathbf{P} = \frac{1}{2\pi}\int dk_x dk_y \, Tr\left[\mathbf{A}(k_x, k_y)\right], \tag{2}$$

where $\mathbf{A}(k_x, k_y) = \langle\psi| i\,\partial_{\mathbf{k}}|\psi\rangle$ is the Berry connection, and the integration is performed over the entire Brillouin zone (BZ). For a system with inversion symmetry, the calculation of P can be substantially simplified by checking the parities of eigenstates at the high symmetry points in the BZ [44]:

$$P_i = \frac{1}{2}\left(\sum_n q_i^n \; modulo2\right), \quad (-1)^{q_i^n} = \frac{\eta(X_i)}{\eta(\Gamma)}\ , \tag{3}$$

where the summation is taken over all the occupied bands and η denotes the parity associated with π rotation, i stands for x or y. Equation (3) indicates the topology of the current PC system is encoded in the parities of Bloch eigenstates at high symmetry points. For example, the eigenstates calculated from finite element simulation and the corresponding eigenvectors at X point on the 3rd branch for configurations A and B are shown in Fig. 1(b). It is easy to find that the parity η associated with π rotation is '-' for configuration A and '+' for configuration B. The difference of parity η implies that the topology of the two configurations are different because the topology depends on the way the unit cell is chosen[21,42,45,46]. By taking all eigenstates at the high symmetry points into account, we obtain $P_A = (0,0)$ and $P_B = (1/2\,, 1/2)$, which means that configuration A is trivial and B is nontrivial.

Recently, people found that in 2D systems the polarization (P_x, P_y) corresponds to the Wannier center of the Bloch state, which is the expectation value of the Wannier function in the real space. The value of $P = p_x^2 + p_y^2$ indicates the distance of the Wannier center from the origin of a lattice site [13,14]. From a topological perspective, the mismatch of the Wannier center with the origin of a lattice site gives rise to second-order boundary state at the corner of the system. These corner states are topologically nontrivial since they have the same origin as the end states in the 1D SSH model. In this way, an analytically solvable tight-binding model with $w = 0$ (or $v = 0$) would offer direct insight for the existence of corner states. For a 2D system with $N \times N$ unit cells as shown in Fig. 1(a), it corresponds to a topologically nontrivial phase with $w = 0$. Among all $4N^2$ sites of the system, there are $4N - 4$ dimers, $(N-1)^2$ tetramers, and 4 isolated

sites. Every dimer occupies energy $\varepsilon_s + v$ and $\varepsilon_s - v$. The tetramer occupies energy $\varepsilon_s \pm v$, and two degenerated energy ε_s. More interestingly, there are 4 isolated sites with energy ε_s, from which 4 corner states can be built. Here we want to point out that the energy of the corner state, ε_s, falls into the energy spectrum of the bulk tetramer states, which means that these corner states are embedded in the continuum. To the best of our knowledge, this is the first observation of nontrivial corner states in the continuum. In contrast, if $v = 0$, the system is in the topologically trivial phase. There are N^2 bulk tetramer states, and no corners states are observed. Thus, we can conclude that the corner states only appear in a topologically nontrivial system.

Although the conditions of $w = 0$ or $v = 0$ are extreme, in the following we will show that the topological properties discussed earlier persist under more relaxed conditions, where neither w nor v is zero. For a $N \times N$ system with $w > v > 0$ (i.e., configuration A), there are $2N$ eigenstates with energy ε_s. We intentionally introduce small random perturbations in the hopping amplitudes and onsite energies to lift the degeneracy of these $2N$ states. We find that the randomly perturbed system has an energy spectrum that preserves the main features of the original periodic system, and no corner states are found. This is consistent with our previous analysis, since configuration A is topologically trivial. In contrast, configuration B ($v > w > 0$) can be adiabatically connected to the extreme case of $w = 0$, thus we expect that the corner states appear in the frequency range of bulk states. This is indeed verified by our calculations. In fact, even after we introduce random perturbations into configuration B, we can still find 4 corner states with energy around ε_s. For a sample of configuration B with $N = 10$, we calculate the frequencies of the eigenstate by using both finite element simulation and tight-binding model, and the results are shown in Fig. 2(b). Both results confirm that the 4 corner states fall into the range of bulk state frequency. The corresponding pressure field distributions given by both the tight-binding model and finite-element simulations are shown in Figs. 2(c) and 2(d), respectively.

In addition to the corner states found in a simple nontrivial system with configuration B, we also find another form of corner state in a more complex composite system consisting of a nontrivial sample surrounded by a trivial sample, as shown in Fig. 3(a). Here we simply set the width of the waveguides connecting the two systems d, representing intersystem hopping, to be identical to d_v , characterizing the intercell hopping in the nontrivial phase (configuration B), i.e., $d = d_v = 5cm$. Four corner states are found at the interface between trivial and nontrivial phases.

All of these four corner states are in the bulk gap region, which differs from the case shown in Fig. 2. The corresponding pressure field distributions for the corner states are obtained by using both the tight-binding model (Fig. 3(c)) and the finite element simulations (Fig. 3(d)). Both results confirm that the fields are highly localized around the four corners of the interface between the trivial and nontrivial phases.

More interesting features of these four corner states are the delocalization and even merging into edge states when the intersystem hopping (denoted as t in the tight-binding model) is tuned [41]. When connecting configuration A with configuration B, we are endowed with some degree of freedom on selecting the intersystem hopping t (or the waveguide width d), as illustrated in Fig. 4(a). Different intersystem hopping leads to different configurations of the corner states as demonstrated in Fig. 4(c). To determine the critical value of t (or d), one can take the following strategy by calculating the projected band structure of a ribbon structure consisting of a nontrivial sample sandwiched between two trivial samples with varying t. There always exists a band gap in the projected band structure except when $t = t_c = 10.8$, which, in our set up, corresponds to the waveguide width $d = d_c = 8.18cm$ in the full wave simulations [41]. From the tight-binding model, it is interesting to find that the size of the band gap depends linearly on $(t - t_c)$ when t deviates from t_c, as shown explicitly in Fig. 4(b). We show the energy spectrum and field distribution at $t = t_c = 10.8$ in the middle panels of Figs. 4(c) and 4(d), respectively, and observe that the corner states merge into the edge state in this case. This is because the band gap vanishes at $t = t_c = 10.8$ and the corner states have to share the same energy with the edge states. In conjunction with the results presented in Fig. 3, it implies that the corner states are not determined solely by the bulk topological invariant, and in some cases, they also depend crucially on the boundary conditions [23]. This finding indicates a new and effective way to manipulate the corner states by simply tuning the intersystem hopping. Figures 4(c) and 4(d) show the energy spectra and field distributions of corner states with different values of t. We observe that the corner states can stay below and isolated from the edge states, then merge into the edge states, and further stay above and isolated from the edge states, as the intersystem hopping t continuously increases.

In conclusion, we find two types of nontrivial corners states in a second-order topological insulator, and interestingly, one type is identified as BIC, which means that they are perfectly

confined without any radiation even when they lie inside the continuum and coexist with extended states. Both types of corner states are found to be associated with the nonzero dipole momentum in the bulk, in contrast with the quantized quadrupole momentum as reported in the literature. We develop a simple tight binding model which can provide analytic solution and direct insight into the origin of the corner states. Full wave simulations based on the realistic acoustic waveguide system are also presented, and together with the tight binding model they corroborate the robustness of the corner states even when random perturbation is introduced. Our findings not only offer an experimentally feasible platform for the study of HOTI in classical wave systems, but also provide an alternative way for the realization of BIC in a simple system. It may stimulate subsequent explorations on the interesting interplay between BIC and HOTI as well as large-area high-power applications in acoustic waves.

Acknowledgement

The work described here are supported by King Abdullah University of Science and Technology Office of Sponsored Research (OSR) under Award No. OSR-2016-CRG5-2950 and Baseline Research Fund BAS/1/1626-01-01, and by the National Natural Science Foundation of China (Grant Nos.11274120 and 11574087).

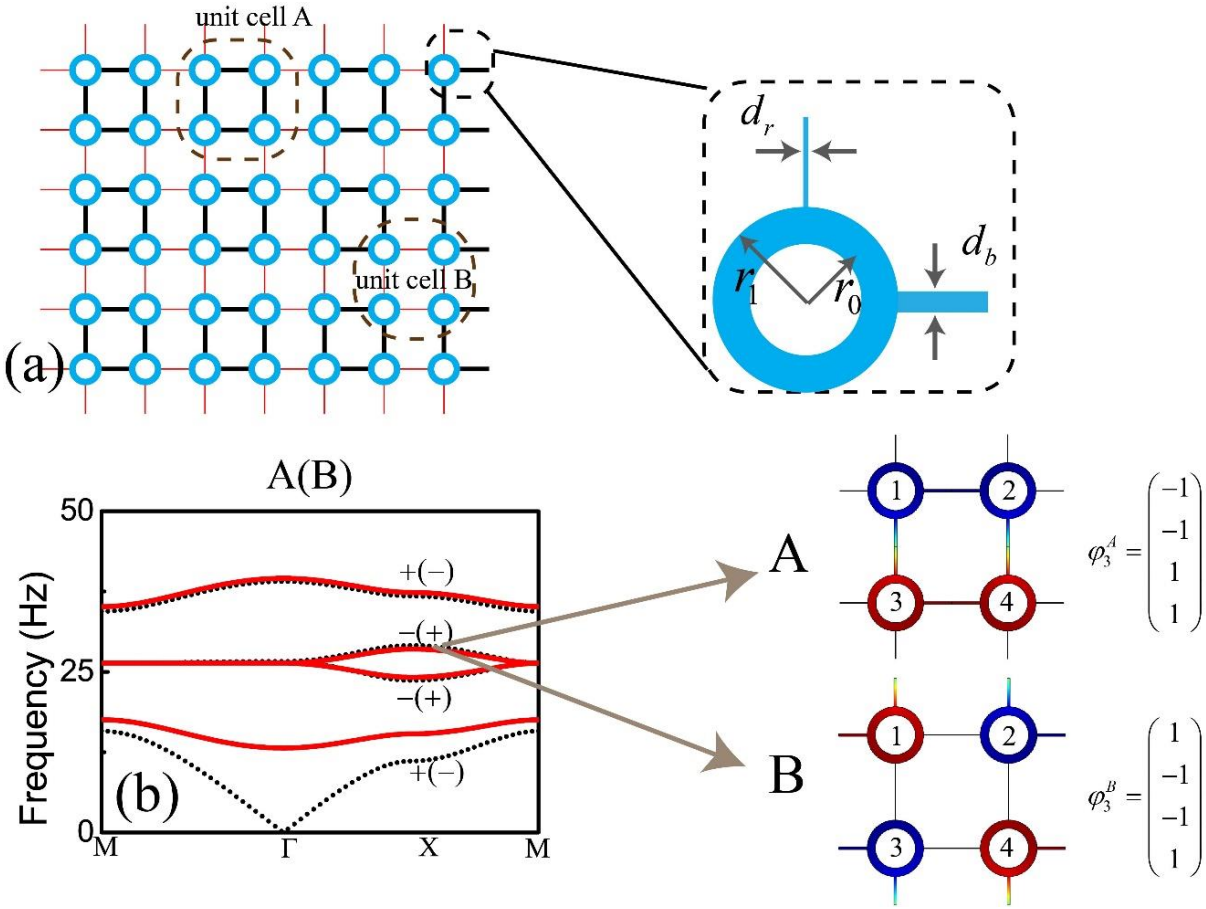

Fig. 1(a) Schematic of the acoustic ring-waveguide system that can be described by the Hamiltonian model, i.e., Eq. (1). Each unit cell contains four identical hollow rings, whose inner and outer radii are fixed, connected by rectangular waveguides. Two different unit cells with inversed intercell and intracell hoppings are circled out. The hopping is characterized by the rectangular waveguides, whose width represents the hopping strength. (b) The calculated band structure using finite element method (black dots), compared with the results obtained from the tight-binding model(red line), where the fitting parameter is $\varepsilon_s = 26.375$, $w = 5, v = 1$. The symbol "$\pm$" means the parity of the states under π rotation, which is derived from the eigenfield distributions and eigenvectors shown in the right inset.

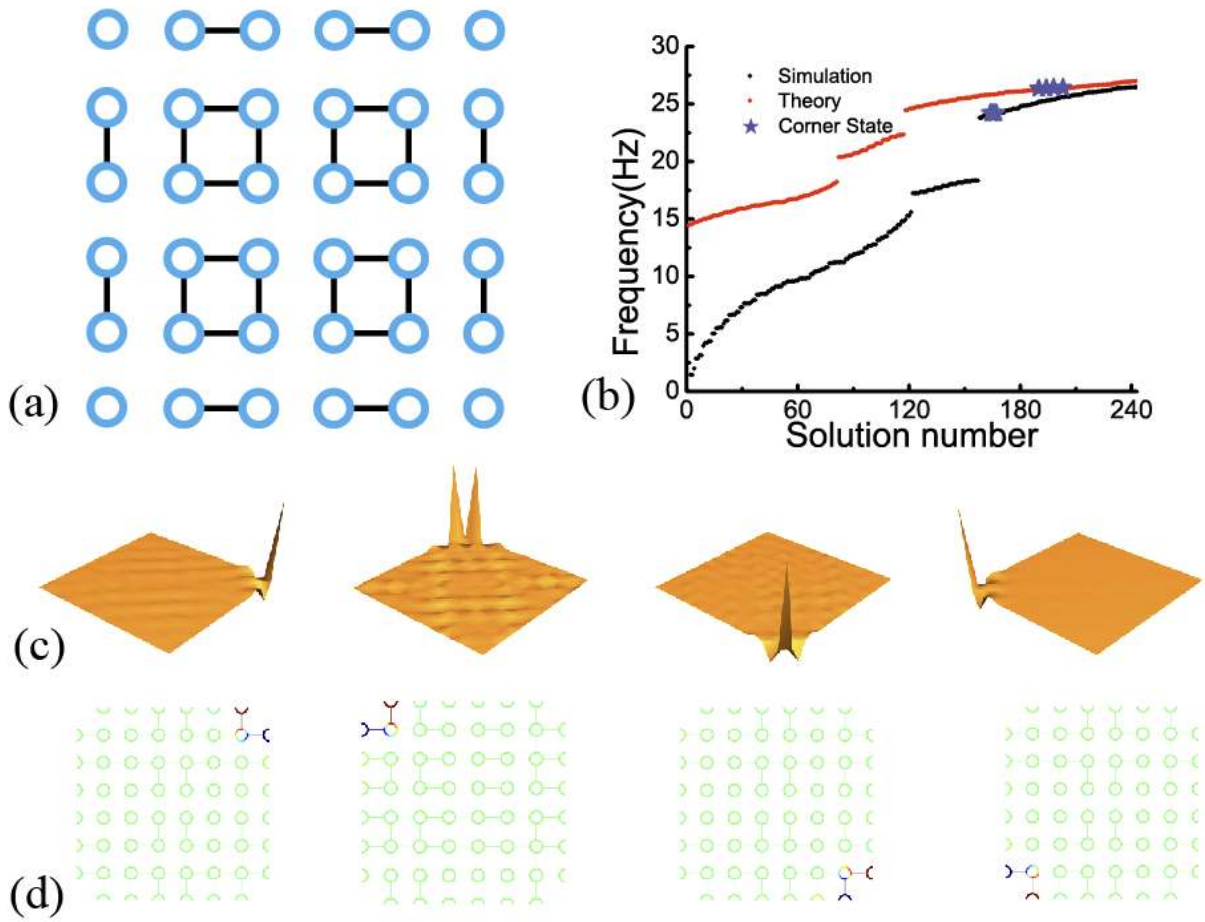

Fig. 2 The corner states in continuum. (a) Illustration of a 3×3 lattice with $w = 0$, the corner states naturally appear. (b) The eigenmodes of a 10×10 sample calculated from both tight-binding model (red point) and numerical simulation result (black point). In the tight-binding model calculations, we introduce small random perturbations to all of the sites energy and coupling parameters. The energy spectrum is plotted after an ensemble average of 10 configurations. The result shows four corner states in the bulk frequency region marked as purple stars. The field distribution of the four corner states from tight-binding model and finite-element simulation are shown in (c) and (d), respectively. The sample size we calculated in (d) is 3×3 for simplicity and clear observation.

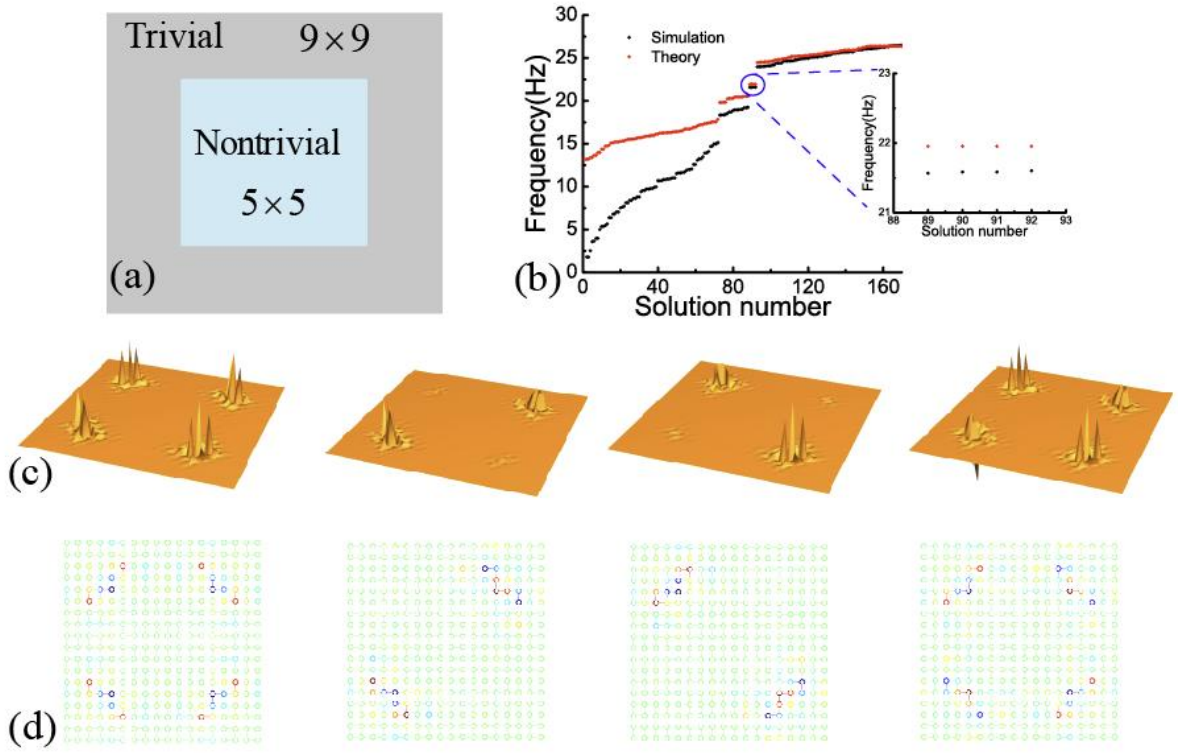

Fig. 3 The corner states in a gap of topological phononic clusters. (a) The sample consists of topologically nontrivial system B surrounded by a topologically trivial system A. (b) The eigenmodes of the sample calculated from both tight-binding model (red point) and finite-element simulation result. We also set the coupling between system A and system B as $t = 5$. The result shows four corner states in the band gap region. (c) and (d) The field distribution of the four corner states from tight-binding model (c) and finite element simulation (d), respectively.

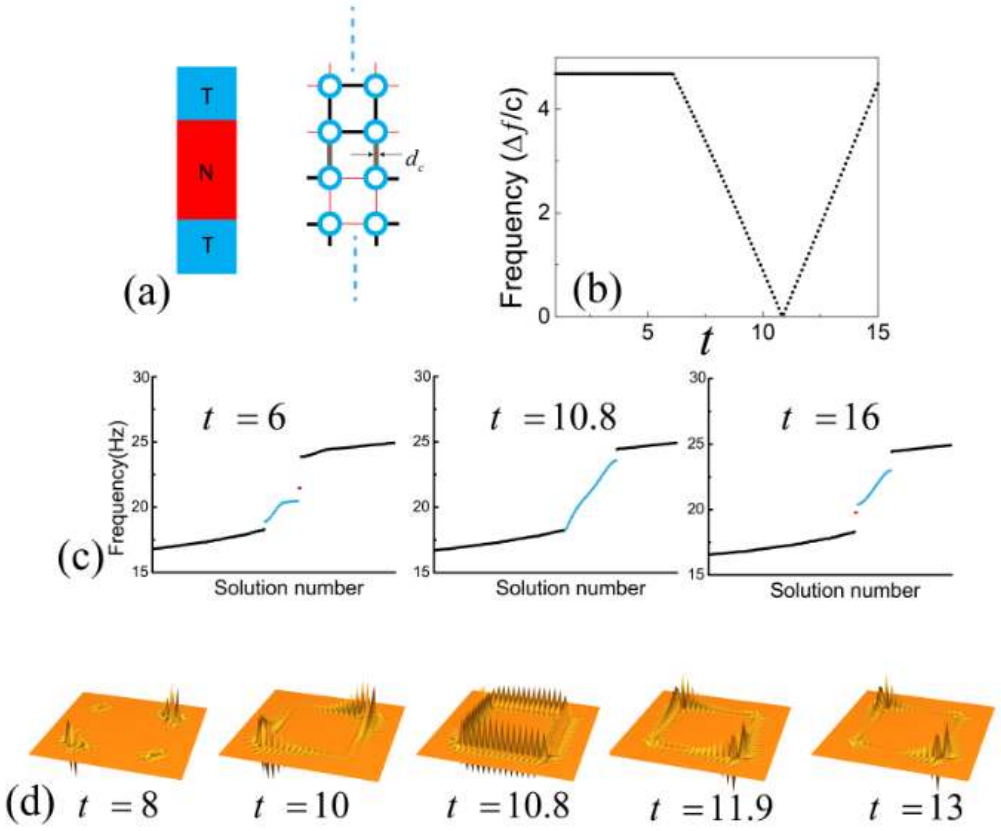

Fig. 4 The corner states evolution against intersystem hopping t. The sample consists 27×27 unit cells. (a) The schematic of a structure that contains two interfaces between system A and system B, where the coupling parameters are undetermined. (b) The estimated band gap size of the edge states as a function of hopping parameters t in the tight binding models. The result indicates there would be a gapless edge state when $t = t_c = 10.8$. (c): The eigenfrequency spectrum of the sample when we change intersystem hopping t. The red points are corner states and the blue points are edge states. (d) The corner states delocalize when the gap of the edge states disappears at certain intersystem hopping $t = t_c = 10.8$.

References

[1] J. E. Moore, Nature **464**, 194 (2010).
[2] M. Z. Hasan and C. L. Kane, Rev. Mod. Phys. **82**, 3045 (2010).
[3] X.-L. Qi and S.-C. Zhang, Rev. Mod. Phys. **83**, 1057 (2011).
[4] C. L. Kane and E. J. Mele, Phys. Rev. Lett. **95**, 226801 (2005).
[5] B. A. Bernevig, T. L. Hughes, and S.-C. Zhang, Science **314**, 1757 (2006).
[6] D. Xiao, W. Yao, and Q. Niu, Phys. Rev. Lett. **99**, 236809 (2007).
[7] K. F. Mak, K. L. McGill, J. Park, and P. L. McEuen, Science **344**, 1489 (2014).
[8] L. Fu, Phys. Rev. Lett. **106**, 106802 (2011).

[9] M. C. Rechtsman, J. M. Zeuner, Y. Plotnik, Y. Lumer, D. Podolsky, F. Dreisow, S. Nolte, M. Segev, and A. Szameit, Nature **496**, 196 (2013).
[10] L. Lu, J. D. Joannopoulos, and M. Soljacic, Nat. Photon. **8**, 821 (2014).
[11] Z. Yang, F. Gao, X. Shi, X. Lin, Z. Gao, Y. Chong, and B. Zhang, Phys. Rev. Lett. **114**, 114301 (2015).
[12] C. He, X. Ni, H. Ge, X.-C. Sun, Y.-B. Chen, M.-H. Lu, X.-P. Liu, and Y.-F. Chen, Nat. Phys. **12**, 1124 (2016).
[13] W. A. Benalcazar, B. A. Bernevig, and T. L. Hughes, Science **357**, 61 (2017).
[14] Z. Song, Z. Fang, and C. Fang, Phys. Rev. Lett. **119**, 246402 (2017).
[15] J. Langbehn, Y. Peng, L. Trifunovic, F. von Oppen, and P. W. Brouwer, Phys. Rev. Lett. **119**, 246401 (2017).
[16] W. A. Benalcazar, B. A. Bernevig, and T. L. Hughes, Phys. Rev. B **96**, 245115 (2017).
[17] F. Schindler, A. M. Cook, M. G. Vergniory, Z. Wang, S. S. P. Parkin, B. A. Bernevig, and T. Neupert, Sci. Adv. **4** (2018).
[18] M. Ezawa, Phys. Rev. Lett. **120**, 026801 (2018).
[19] C. W. Peterson, W. A. Benalcazar, T. L. Hughes, and G. Bahl, Nature **555**, 346 (2018).
[20] S. Imhof *et al.*, Nat. Phys. **14**, 925 (2018).
[21] B.-Y. Xie, H.-F. Wang, H.-X. Wang, X.-Y. Zhu, J.-H. Jiang, M. H. Lu, and Y. F. Chen, Phys. Rev. B **98**, 205147 (2018).
[22] X. Zhang, H.-X. Wang, Z.-K. Lin, Y. Tian, B. Xie, M. H. Lu, Y.-F. Chen, and J.-H. Jiang, arXiv:1806.10028 (2018).
[23] H. Xue, Y. Yang, F. Gao, Y. Chong, and B. Zhang, Nat. Mater. (2018).
[24] X. Ni, M. Weiner, A. Alù, and A. B. Khanikaev, Nat. Mater. (2018).
[25] M. Serra-Garcia, V. Peri, R. Süsstrunk, O. R. Bilal, T. Larsen, L. G. Villanueva, and S. D. Huber, Nature **555**, 342 (2018).
[26] C. W. Hsu, B. Zhen, A. D. Stone, J. D. Joannopoulos, and M. Soljačić, Nature Reviews Materials **1**, 16048 (2016).
[27] J. Lee, B. Zhen, S.-L. Chua, W. Qiu, J. D. Joannopoulos, M. Soljačić, and O. Shapira, Phys. Rev. Lett. **109**, 067401 (2012).
[28] M. Robnik, Journal of Physics A: Mathematical and General **19**, 3845 (1986).
[29] H. Friedrich and D. Wintgen, Phys. Rev. A **32**, 3231 (1985).
[30] F. Remacle, M. Munster, V. B. Pavlov-Verevkin, and M. Desouter-Lecomte, Phys. Lett. A **145**, 265 (1990).
[31] K. Hirose, Y. Liang, Y. Kurosaka, A. Watanabe, T. Sugiyama, and S. Noda, Nat. Photon. **8**, 406 (2014).
[32] M. Meier, A. Mekis, A. Dodabalapur, A. Timko, R. E. Slusher, J. D. Joannopoulos, and O. Nalamasu, Appl. Phys. Lett. **74**, 7 (1999).
[33] S. Noda, M. Yokoyama, M. Imada, A. Chutinan, and M. Mochizuki, Science **293**, 1123 (2001).
[34] A. A. Yanik, A. E. Cetin, M. Huang, A. Artar, S. H. Mousavi, A. Khanikaev, J. H. Connor, G. Shvets, and H. Altug, Proc. Natl. Acad. Sci. **108**, 11784 (2011).
[35] B. Zhen, S.-L. Chua, J. Lee, A. W. Rodriguez, X. Liang, S. G. Johnson, J. D. Joannopoulos, M. Soljačić, and O. Shapira, Proc. Natl. Acad. Sci. **110**, 13711 (2013).
[36] J. M. Foley, S. M. Young, and J. D. Phillips, Phys. Rev. B **89**, 165111 (2014).
[37] Y.-X. Xiao, G. Ma, Z.-Q. Zhang, and C. T. Chan, Phys. Rev. Lett **118**, 166803 (2017).
[38] Y. Yang, Z. Yang, and B. Zhang, J. Appl. Phys. **123**, 091713 (2018).
[39] Z.-G. Chen and Y. Wu, Phys. Rev. Appl. **5**, 054021 (2016).
[40] Z.-G. Chen, J. Zhao, J. Mei, and Y. Wu, Sci. Rep. **7**, 15005 (2017).
[41] See Supplemental Material for discussion of the realistic acoustic waveguide structures used in Fig. 2d, the robustness of the corner states and the gapless edge state dispersion in the real structures.

[42] F. Liu and K. Wakabayashi, Phys. Rev. Lett. **118**, 076803 (2017).
[43] R. Resta, Rev. Mod. Phys. **66**, 899 (1994).
[44] C. Fang, M. J. Gilbert, and B. A. Bernevig, Phys. Rev. B **86**, 115112 (2012).
[45] M. Xiao, G. Ma, Z. Yang, P. Sheng, Z. Q. Zhang, and C. T. Chan, Nat. Phys. **11**, 240 (2015).
[46] K. H. Choi, C. W. Ling, K. F. Lee, Y. H. Tsang, and K. H. Fung, Opt. Lett. **41**, 1644 (2016).